Spectroscopic Observation of Isomerization Kinetics in Isotopically Labeled (Benzene)$_{13}$

David C. Easter,* Jennifer P. Harris, Matt Langendorf, James Mellott, Michael Neel, and Todd Weiss

Department of Chemistry, Southwest Texas State University, San Marcos, Texas 78666

Received: September 9, 1998; In Final Form: October 2, 1998

Isotopically labeled (benzene)$_{13}$ clusters, $(C_6H_6)(C_6D_6)_{12}$, generated in supersonic expansion, were studied by resonance-enhanced two-photon ionization (R2PI) spectroscopy as a function of nozzle-to-laser distance using two distinct sets of expansion conditions. In this report we present spectroscopic evidence for both evaporation and isomerization within the supersonic jet. The observed $(C_6H_6)(C_6D_6)_{12}$ population initially undergoes a fluxional-to-rigid transition; this transition is followed by isomerization within a subpopulation of the ordered, rigid clusters, in which the unique C_6H_6 moiety migrates *from the surface to the interior* of an otherwise homogeneous C_6D_6 cluster. These experiments are unique in that analogous isomerization dynamics have never before been spectroscopically observed. The observed kinetics are generally insensitive to differences between the benzene:helium ratio in the expansion mixture.

I. Introduction

Size-selected clusters have often been studied to probe fundamental properties and dynamics within finite systems. In principle, a unique molecular chromophore, when embedded in a cluster and probed spectroscopically, provides data that may lead to the identification of the structure and the dynamical processes that occur in the chromophore's local environment.

Resonance-enhanced two-photon ionization (R2PI) spectroscopy has proven to be a successful tool for the study of benzene clusters. Smalley et al. introduced the application of this technique to small benzene clusters several years ago.[1] Subsequently, Schlag and co-workers reported R2PI experiments, focusing primarily on (benzene)$_2$ and (benzene)$_3$.[2,3,4] Using the technique of isotopic labeling, they explored the nature of the intermolecular interactions within the dimer, trimer, and tetramer clusters, and used spectroscopic data to infer cluster structures based on a weak-interaction model. The structure of the benzene dimer has also been investigated by Felker, et al., using stimulated Raman spectroscopy.[5]

From the theoretical perspective, both Williams[6] and van de Waal[7,8] have computed structures for small benzene clusters. Their calculations involve minimization of the cluster's potential energy, derived from intermolecular atom−atom pair-potential functions. Both calculations for (benzene)$_{13}$ yield a quasi-icosahedral structure, in which the twelve surface molecules are divided into two symmetry-distinct sets, each set having six members.

Several studies of fluxional-rigid transitions within finite-sized clusters have been reported. The (benzene)Ar$_n$ system has been a common focus for both experimentalists and theoreticians, particularly because of the system's promise for correlating theory with experiment. Hahn and Whetten introduced the first potential evidence for such a transition based on (C_6D_6)-Ar$_n$ ultraviolet spectra;[9] Adams and Stratt have undertaken extensive theoretical studies on the "phase" question in benzene-argon clusters;[10,11] further results of spectroscopic studies have been published by Felker et al.,[12] Knochenmuss et al.,[13] and Easter et al.[14]

Easter and co-workers have experimentally investigated fluxional-rigid transitions in $(C_6H_6)(C_6D_6)_{12}$,[15,16] while Bartell et al. have studied the (benzene)$_{13}$ system by Monte Carlo simulation.[17,18] In earlier work, Bartell et al. originally approached the experimental investigation of phase in very large benzene clusters using electron diffraction techniques;[19] in most cases they found that clusters in their supersonic flow revealed a local molecular order indicative of supercooled bulk liquids.[20] In addition, the (benzene)$_4$ cluster has been the focus of a theoretical study by Stace et al.[21]

Spectroscopic experiments have proved the possibility of generating benzene clusters with a significant fraction in stable, rigid isomeric forms. Under favorable conditions, supersonic cluster jets contain a few, at most, significant rigid isomers of (benzene)$_n$, $n = 12-15$.[22,23,24] In isotopically labeled studies (when the clusters are interrogated 1000 nozzle diameters from the expansion origin), it is observed that a single, sharp feature dominates the $B_{2u} \leftarrow A_{1g}$ 6^1_0 absorption when the chromophore, C_6H_6, is monitored in cold $(C_6H_6)(C_6D_6)_{n-1}$ clusters ($n = 12-19$). For each of these cluster sizes, the sharp feature originates from a C_6H_6 chromophore localized in the cluster's interior site.[24]

An experiment reported by Easter, Baronavski, and Hawley took advantage of the simplicity of this spectrum and monitored its evolution as a function of expansion time.[16] The first experimental evidence for a fluxional-rigid transition in a single size molecular cluster was presented in that report. In the first 50 μs of expansion, the (benzene)$_{13}$ cluster population underwent transformation, from being entirely nonrigid to having a substantial population in rigid form.

The data presented in this report significantly extend previously reported results. The laser-to-nozzle distance range in these experiments has been extended by a factor of 4 compared with the studies in ref 16: from a maximum of 184 to 804 D, where D represents one nozzle diameter (0.50 mm). Here we present, under two sets of expansion conditions, spectroscopic evidence for isomerization within a subpopulation of the rigid (benzene)$_{13}$ cluster.

10.1021/jp983650m CCC: $15.00
Published on Web 11/14/1998

II. Experimental Approach

Neutral $(C_6H_6)(C_6D_6)_n$ clusters are formed by free jet expansion through a pulsed molecular beam valve (R. M. Jordan C-211) into high vacuum (background 10^{-7} Torr), using a 0.50 mm diameter valve orifice, and a conically diverging nozzle (30° measured wall-to-wall, 3 mm length). The benzene−helium expansion mixture is created by flowing He (10 atm) through the benzene sample, with the valve at ambient temperature. Two sets of data are collected. For the first, the benzene solution is at 298 K (He:benzene = 120); for the second, the sample is maintained at 273 K (He:benzene = 360). The benzene sample is a 5% solution of C_6H_6 in C_6D_6, which is statistically expected to generate a ratio, $(C_6D_6)_{13}$:$(C_6H_6)(C_6D_6)_{12}$:$(C_6H_6)_2(C_6D_6)_{11}$:$(C_6H_6)_3(C_6D_6)_{10}$, of 51:35:11:2. Because the experiments are undertaken in a regime where the C_6D_6 molecule is spectroscopically transparent (−250 to −140 cm^{-1} shift, relative to the C_6H_6 molecular resonance at 38608.5 cm^{-1}), the relevant $(C_6H_6)(C_6D_6)_{12}$:$(C_6H_6)_2(C_6D_6)_{11}$:$(C_6H_6)_3(C_6D_6)_{10}$ ratio is 72:23:4. (The molecular $C_6H_6-C_6D_6$ isotope shift is 179 cm^{-1}; the same shift is observed between $(C_6H_6)_{13}$ and $(C_6D_6)_{13}$ clusters.[23]) The $(benzene)_{13}$ mass peak is windowed such that intensity of the latter 70% of the peak is recorded. Although it is likely that some contribution from $(C_6H_6)_2(C_6D_6)_{11}$ remains, it is reasonable to estimate that more than 90−95% of the collected signal derives specifically from $(C_6H_6)(C_6D_6)_{12}$. Any $(C_6H_6)_2(C_6D_6)_{11}$ present will affect the spectra by causing an overestimation of the integrated area of feature B, described below (see ref 24).

The gas mixture expands supersonically into the vacuum chamber, and passes, at a variable distance downstream, unskimmed through the extraction plates of a time-of-flight mass spectrometer (R. M. Jordan C-677). The time-of-flight (TOF) extraction plates are configured such that the TOF axis is perpendicular to both the cluster beam and the laser beam. Each 10 Hz pulse of the valve signals the digital delay generator (Stanford DG535), which synchronizes the laser and the oscilloscope. The required wavelength (∼260 nm) is produced by generating the second harmonic of a YAG-pumped dye laser (Lambda Physik LPY 150, ScanMate2C, BBO I) operating on coumarin 503. The laser ionizes the clusters through the $B_{2u} \leftarrow A_{1g}$ 6^1_0 vibronic transition of the C_6H_6 moiety via a one-color 1+1 multiphoton ionization scheme.

Cluster fragmentation is expected to have some effect on the one-color data presented in this study. In preparation for these experiments, we tested for such fragmentation by simultaneously measuring the spectra of $(C_6H_6)(C_6D_6)_{12}$ and $(C_6H_6)(C_6D_6)_{13}$ at an expansion distance of 840 nozzle diameters (42 cm), with the benzene sample at −15 °C, at a scan step size of 0.35 cm^{-1}, and over a limited spectral range: −240 to −200 cm^{-1} shift. The results, shown in Figure 1 (left), compare favorably with fragmentation-free two-color spectra (ref 24), and show very little evidence of fragmentation. On the basis of these exploratory spectra, we estimate that no more than 5−10% of the signal recorded in the $(benzene)_{13}$ mass channel originates from higher clusters, primarily $(benzene)_{14}$. Fortunately, a small amount of fragmentation does not negatively impact the results. Previous experiments have established that the spectra of $(C_6H_6)(C_6D_6)_{12}$, $(C_6H_6)(C_6D_6)_{13}$, and $(C_6H_6)(C_6D_6)_{14}$ all have important commonalities: all have a prominent feature near −220 cm^{-1} that derives from the cluster's interior site, and their spectral shifts differ from each other by no more than a few wavenumbers.[24] Because the dynamics are qualitatively similar for all cluster sizes in this region, the presence of a small amount of fragmentation does not significantly affect either the analysis or the interpretation.

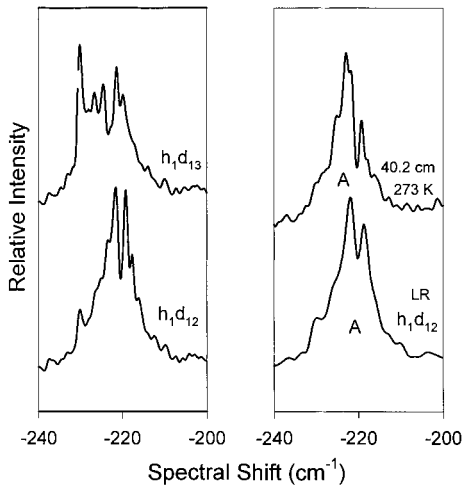

Figure 1. (Left). Exploratory one-color spectra of $(C_6H_6)(C_6D_6)_{12}$ and $(C_6H_6)(C_6D_6)_{13}$, labeled h_1d_{12} and h_1d_{13}. These are collected over a narrow spectral range (−240 cm^{-1} to −200 cm^{-1} shift), at a scan-step limited resolution of 0.35 cm^{-1}, and with the benzene solution at −15 °C. These compare favorably with fragmentation-free two-color spectra (ref 24). (Right). Direct comparison of a lower resolution rendition of the exploratory $(C_6H_6)(C_6D_6)_{12}$ spectrum (bottom) with data from the 40.2 cm (273 K) spectrum in the same wavenumber region (top).

R2PI spectra are generated by sequentially stepping the grating of the dye laser while, at each wavelength, averaging the ion signal (normalized by the square of the laser intensity) over mass-specific windows, using a digital oscilloscope (LeCroy 9310AM). Spectra are obtained by recording the normalized ion intensity (averaged over 75 laser shots) at each wavelength. The spectral resolution is limited by scan step size (0.75 cm^{-1}). The experimental process is controlled by PC-based data acquisition software, operating on a Windows-based LabView (National Instruments) platform. Several scans are recorded at the same distance with the benzene sample at 298 K and the average is reported; the benzene sample is then cooled to 273 K, and the system is allowed to equilibrate before three or more additional data scans are collected. The experimental setup requires that scans taken at different distances be recorded on different days.

Figure 2 presents the velocity profile for $(benzene)_{13}$ in the jet, demonstrating that the clusters are expanding with the velocity of a neat helium free jet. The delay time (μs) is plotted vs nozzle-to-laser distance (cm); the distance, in units of nozzle diameters, D, is indicated on the top axis. The delay (between the nozzle and laser-trigger pulses) is optimized to maximize the $(benzene)_{13}$ signal. The $(benzene)_{13}$ clusters are detected only in the highest density regions of the free jet pulse, and the observed fwhm of the $(benzene)_{13}$ packet is 6 μs, compared to the total gas pulse fwhm of 35 μs. (The timing jitter between the nozzle and laser triggers is ∼100 ps.) Experimental errors associated with the delay time (±3 μs, corresponding to 50% of the fwhm of the $(benzene)_{13}$ cluster packet) and the nozzle-to-laser distance (±0.25 cm) form the boundaries for each data point in Figure 2. The data are fit to the linear expression, $t^* = d/v + t_o$, where d is the experimental nozzle-to-laser distance in the expansion, t^* is the optimized delay time between the nozzle and laser triggers, v is the velocity of the center of the $(benzene)_{13}$ packet, and t_o is a constant specific to the machine. The slope is determined to be 5.18 ± 0.05 μs/cm, with a regression coefficient, $r^2 = 0.9994$. The expansion time for the center of the cluster packet center is then taken to be $t = d/v$, shown on the right axis of Figure 2. Because the arrival time of the $(benzene)_{13}$ cluster packet is so narrow at all nozzle-to-

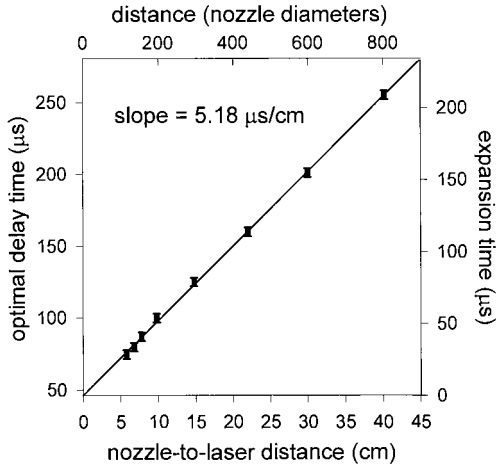

Figure 2. Velocity profile for $(benzene)_{13}$ in the helium free-jet expansion. The profile is determined by measuring the optimal delay time between the pulsed valve and the laser trigger at the nozzle-to-laser distances used in the experiment. Uncertainties in distance (0.25 cm) and time (3 μs) are reflected by the size of the data points. (The uncertainty in time is taken to be 50% of the cluster packet's fwhm; this is distinct from the timing jitter, ~100 ps.) The right axis indicates the expansion distance in units of nozzle diameters (D), and the top axis indicates the expansion time of the $(benzene)_{13}$ packet.

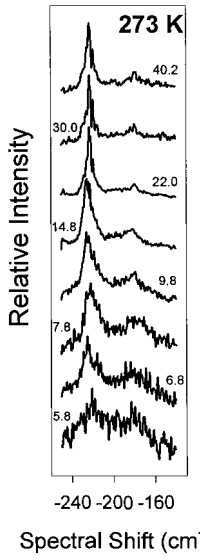

Figure 3. Experimental data for spectra collected at each of eight nozzle-to-laser distances, with the benzene sample at 273 K. The expansion distance (in cm) identifies each spectrum.

laser distances, (there is no measurable broadening as the expansion distance increases), the rate of expansion is known within 1%.

This expansion rate corresponds to a velocity of 1930 ± 20 ms^{-1}. This magnitude is somewhat surprising in light of theoretical calculations that identify the terminal velocity of neat helium expansions either as 1360 ms^{-1} or 1760 ms^{-1}.[25,26] It is worth noting that empirical measurements have demonstrated that expansion velocities increase in some fashion as the stagnation pressure is increased: specifically, a velocity of 400 ms^{-1} is reported with a stagnation pressure of 1 atm,[27] 1360 ms^{-1} at 5 atm,[25] 1780 ms^{-1} at 7 atm,[26] and 1900 ms^{-1} at 9 atm.[15] (Within experimental error, our present measurement is identical to the latter.) Our attempts to devise a compelling theoretical argument for the observed velocity have thus far fallen short; nevertheless, the independent experimental measurements referenced above demonstrate that the helium free jet velocity increases in some way with stagnation pressure, at least to pressures of 9 atm.

III. Experimental Results

Figure 3 shows the spectra of $(C_6H_6)(C_6D_6)_{12}$ corresponding to eight different nozzle-to-laser distances with benzene at 273 K; Figure 4 shows the same series of distances with the sample at 298 K. In each spectrum, relative intensity is plotted vs spectral shift from the 6^1_0 C_6H_6 molecular resonance (38608.5 cm^{-1}). Each of the eight spectra, represented by the data points in Figure 4, consists of exactly three features: feature A, a sharp absorption near -220 cm^{-1} shift, which originates from the rigid cluster's interior molecule;[23,24] feature B, a second sharp feature near -180 cm^{-1} shift, which originates from C_6H_6 on the rigid cluster's surface;[22,24] and feature C, a broad underlying absorption originating from $(C_6H_6)(C_6D_6)_{12}$ clusters in a fluxional state and/or in multiple disordered isomeric forms.[16]

Because the similarities between the exploratory spectrum, h_1d_{12} (Figure 1, left, bottom) and the data presented in Figures 3 and 4 may not be immediately obvious, we provide a direct comparison between the two in Figure 1 (right), where the spectral range plotted is limited to -240 to -200 cm^{-1} shift, i.e., in the vicinity of feature A. The data collected at 40.2 cm (273 K) are presented as a solid line in the upper trace, and a lower-resolution reproduction of the h_1d_{12} exploratory spectrum is reproduced in the lower trace. This is generated by sequentially pairing and averaging data in the original h_1d_{12} exploratory spectrum; in effect, this reduces the number of data points by 50%, resulting in an effective resolution similar to that of the 40.2 cm data. Direct comparison reveals that differences between the two are limited to the fine structure of feature A. These may be attributed to different (benzene:helium) ratios in the two expansions (~3 times larger in the 40.2 cm data, compared to the exploratory spectrum) and to different laser-to-nozzle distances.

Qualitative trends observed in the spectra as a function of nozzle-to-laser distance include: (i) narrowing of the two sharper features (A and B) as the distance is increased, each having a minimum Gaussian width of ~4 cm^{-1}; (ii) an increase in the integrated area of feature A relative to that of feature B; and (iii) a decrease in the relative area of feature C over a short distance range (116−200 D), with a leveling out at further distances.

IV. Analysis and Discussion

A. Spectral Deconvolution. Given appropriate expansion conditions, it has been shown that benzene clusters in the 13 molecule range are produced and detected with a significant fraction in rigid isomeric forms; the resulting electronic spectra yield specific, reproducible features.[22−24] Previously reported spectra are consistent with a quasi-icosahedral geometry for $(benzene)_{13}$, as predicted by van de Waal.[8] A single interior molecule with lower than C_3 symmetry is solvated by two structurally distinct sets of surface molecules; each set contains six members. The clusters presumably exist in two enantiomeric forms, the "average" of which yields local C_3 symmetry for the cluster interior. Isotopically labeled studies of (C_6H_6)-$(C_6D_6)_{12}$, in which only the C_6H_6 moiety is probed 1000 D from the expansion origin, reveal a dominant sharp feature near -220 cm^{-1} shift, assigned to C_6H_6 in the cluster interior (feature A), and a second sharp but less intense feature near -180 cm^{-1}, assigned to C_6H_6 on the cluster surface (feature B). The assignment of these two features is supported by the spectrum

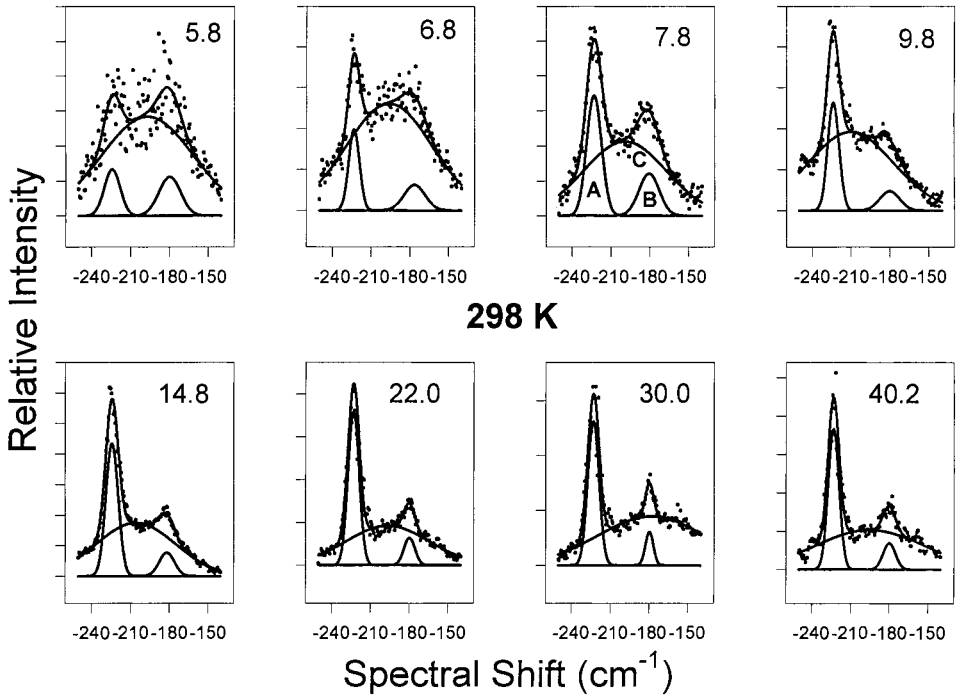

Figure 4. Experimental data and their mathematical fits for spectra collected with the sample at 298 K. The expansion distance (in centimeters) is shown in the upper right corner of each spectrum. Each spectrum monitors the C_6H_6 moiety's absorption within a $(C_6H_6)(C_6D_6)_{12}$ cluster and is plotted as relative intensity vs spectral shift relative to the C_6H_6 molecule's gas phase 6^1_0 absorption at 38608.5 cm^{-1}. Experimental data is represented by dots. Three Gaussian features (labeled A, B, and C in the 7.8 cm plot) comprise each spectrum. The solid line through the data represents the sum of the three features. The position, width, and integrated area of each Gaussian feature are determined by a best fit to the data.

of $(C_6H_6)_2(C_6D_6)_{11}$, which has two corresponding sharp features of nearly equal intensity.[24] A broad feature underlying the two sharp features is inferred from all the neat benzene spectra and is observed in all isotopically labeled cluster studies (feature C). Easter, Baronavski, and Hawley argued that this feature can be interpreted as the manifestation of disordered, fluxional clusters.[16]

Because the $(C_6H_6)(C_6D_6)_{12}$ spectra measured at all eight nozzle-to-laser distances used in this experiment are well described as a sum of the three previously assigned features described above, we have determined the best fit to each experimental trace based on a sum of the three corresponding Gaussian waveforms, using the curve fitting routine in Jandel Scientific's SigmaPlot. For each Gaussian, we determined the integrated peak area α, the mean spectral shift μ, and the width σ. Results of those fits are incorporated into Figure 4. In all cases, feature A is found at a mean spectral shift of -223.2 ± 1.1 cm^{-1} and feature B is at -179.8 ± 1.6 cm^{-1}. Feature C, the broad feature, is centered at -198 ± 9 cm^{-1}, with a width of 38 ± 5 cm^{-1}. Positions of the two sharp features are in excellent agreement with previous reports;[16] however, feature C is shifted 40 cm^{-1} to the red and is only half as broad as reported in ref 16. The differences may be related to a couple of factors: the previous experimental design employed a different molecular beam valve and used slightly different expansion conditions; in addition, previously reported spectra were complicated by interference from C_6D_6 absorption, because they did not exclude the range spanning from -140 cm^{-1} shift to -120 cm^{-1} shift, where C_6D_6 is not spectroscopically transparent.

B. Evaporation Kinetics: **The Evolution of Feature C.** The fluxional-rigid transition in $(benzene)_{13}$ has already been experimentally observed;[15] Bartell's Monte Carlo studies have placed this interpretation of the data on solid theoretical ground, verifying that the fluxional-rigid transition in $(benzene)_{13}$ should be observable by spectroscopic measurements.[18] In the same analysis, Bartell draws the conclusion that evaporation (not cluster collisions with the carrier gas) is responsible for effecting the transition. One motivation for the present study was to expand the dynamical range of the report in ref 16. Our present data confirms the early-time evolution in feature C; however, the evolution of this feature at expansion distances beyond 15 cm (300 D) cannot be described by extrapolation of the simple first-order decay, determined by the 0−200 D data. Bartell's contention, coupled with our most recent data, have drawn us to the conclusion that evaporation is central to the mechanism underlying the fluxional-rigid transition observed within the first 300 D of expansion.

To evaluate the time dependence of feature C's relative integrated intensity, we consider the following evaporation reactions:

	evaporation reaction	affect on feature C
(i)	(HD_{14}) flux → (HD_{13}) flux + D	none
(ii)	(HD_{13}) flux → (HD_{12}) flux + D	increase
(iii)	(HD_{12}) flux → $(benzene)_{12}$ products + (H or D)	decrease
(iv)	(HD_{13}) flux → (HD_{12}) rigid, disordered + D	increase

The effect of each elementary reaction on the integrated intensity of feature C, the broad feature in the 13-cluster mass channel, is indicated to the right. Reactions i and ii represent a sequence in which a fluxional cluster of a specific size loses one C_6D_6 molecule, producing a fluxional cluster of the next lower size. Reaction iii represents the evaporation of fluxional $(benzene)_{13}$, without respect to the products of evaporation. Reaction iv represents evaporation of a monomer from fluxional $(benzene)_{14}$ resulting in an assortment of rigid, but disordered (C_6H_6)-$(C_6D_6)_{12}$. The latter are stable to further evaporation because the cluster's closed-shell configuration implies a large activation

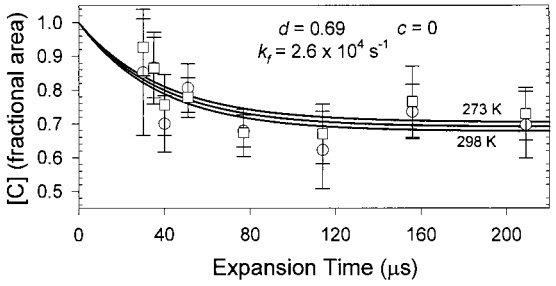

Figure 5. Plot of the fractional area of Feature C vs expansion time. The 298 K data is represented by circles, 273 K data by squares. The best fits to the model described in the text are shown. The 273 K data fit is the upper line and the 298 K fit is the lower line; a fit to the combined data is represented by the center line. Derived parameters for the combined data are $c = 0$, $d = 0.69$, and $k_f = 2.6 \times 10^4\ s^{-1}$; these values for c and d imply that evaporation of a monomer from fluxional $(benzene)_{14}$ results almost exclusively in rigid $(benzene)_{13}$ clusters, the majority of which are disordered.

energy. (See further discussion in section C of this report.) Furthermore, the contribution of these rigid, disordered clusters to the $(C_6H_6)(C_6D_6)_{12}$ spectrum will be broad, and spectroscopically indistinguishable from their fluxional counterparts. As a result, feature C is interpreted as a spectroscopic superposition of both fluxional and rigid, disordered $(benzene)_{13}$ clusters.

To derive an analytical expression for the relative integrated intensity of feature C as a function of time, we employ three assumptions: (1) neighboring cluster sizes have nearly equal initial populations; (2) evaporation from fluxional clusters of neighboring cluster sizes occurs at nearly equal rates; and (3) given fixed expansion conditions, the stoichiometric ratio of evaporation products is constant. The first assumption is supported by nearly equal intensities of neighboring-sized clusters, both in the mass spectra and the optical spectra.

The stoichiometric ratios, (a, b, c, and d) are defined by the following evaporation reaction:

$$(HD_{13})\text{flux} \rightarrow a[H][D_{12}] + b[D][HD_{11}] + c(HD_{12})\text{flux} + d\{HD_{12}\}\text{rigid, disordered} + C_6D_6 \quad (1)$$

Specifically, c represents the probability that evaporation of fluxional $(HD_{13})_{flux}$ cluster will yield a fluxional HD_{12} cluster, (HD_{12})flux, upon evaporation of C_6D_6, while d represents the probability that the product will be a rigid, disordered 13-cluster, $\{HD_{12}\}$rigid, disordered. In this equation, the notation, $[H][D_{12}]$, indicates a highly ordered, rigid cluster with C_6H_6 in the cluster interior, while $[D][HD_{11}]$ denotes an ordered, rigid cluster with C_6D_6 in the interior, and therefore, the unique C_6H_6 chromophore is located within the first solvation shell, (i.e., on the cluster surface).

The derived analytical expression for the time-dependence of the relative integrated intensity of Feature C is given by

$$\frac{[C] + [D]}{[C]_0} = \frac{d}{1-c} + \left(1 - \frac{(d)}{(1-c)}\right)\exp(-(1-c)k_f t) \quad (2)$$

where [C] represents the concentration of (HD_{12})flux, [D] represents $\{HD_{12}\}$rigid, disordered, and $[C]_0$ represents the initial concentration of fluxional $(C_6H_6)(C_6D_6)_{12}$. The term on the left side of the equality represents the relative integrated intensity of feature C; k_f represents the first-order rate constant for evaporation of fluxional benzene clusters in the 13-molecule cluster size range; c and d are the ratios defined in eq 1.

A best-fit of the data to eq 2 is shown in Figure 5, where the fractional area (integrated intensity) of Feature C is plotted vs expansion time (microseconds). The 298 K data are represented by circles and the 273 K data by squares. Three fits are shown: the upper line represents a fit to only the 273 K data, the lower line corresponds to the 298 K data, and the middle line is a fit to the combined data. Although there are small differences between the two temperature-specific fits, experimental uncertainties are large enough that putting any emphasis on those differences is unwarranted. These results indicate that the experimental kinetics are generally insensitive to the differences between two sets of expansion conditions that differ in their benzene:helium expansion ratios by a factor of 3. Consequently, all discussion that follows is based on the combined results.

The analysis underlying Figure 5 leads to the conclusion that *nearly all* evaporations from fluxional $(benzene)_{14}$ result in rigid $(benzene)_{13}$, i.e., $c \approx 0$, that the evaporative rate constant, $k_f = 2.6 \times 10^4\ s^{-1} \pm 0.7 \times 10^4\ s^{-1}$, and that the fraction of fluxional clusters solidifying into rigid, disordered clusters, $d = 0.69 \pm 0.03$. In subsequent calculations these values will be used without modification.

To estimate a temperature for this evaporation-driven transition, we use the rate constant formalism derived by Klots:[28,29]

$$k_{evap}(T)(s^{-1}) = (3 \times 10^{13} n^{2/3})\exp(6/n^{1/3})\exp(-\Delta E_a(n)/k_B T) \quad (3)$$

In this expression, n represents the number of molecules in the cluster, and $\Delta E_a(n)$ is the Arrhenius activation energy, related in the hard sphere model to the energy of evaporation by

$$\Delta E_a = \Delta E_{evap} + {}^1/_2 k_B T \quad (4)$$

Using the energies of rigid $(benzene)_{12}$, $(benzene)_{13}$, and $(benzene)_{14}$ as calculated by Bartell and Dulles, -284.209, -324.915, and -352.903 kJ/mol, respectively,[17] the experimental evaporation temperature is found to be 137 K. This is in good agreement with Bartell's theoretically determined temperature of 140 K for the fluxional-rigid transition.[18]

In summary, the solidification process observed in the $(benzene)_{13}$ mass channel within the first 200 D of expansion, is driven by evaporation of $(benzene)_{14}$ at a temperature near 137 K. While virtually all fluxional $(benzene)_{14}$ cluster evaporations result in the formation of rigid $(benzene)_{13}$, the data reveal that a significant percentage (69%) of the product rigid clusters are, in fact, disordered.

C. The Evolution of Feature B: Evaporation or Isomerization? For the purpose of discussion, we define the fraction f by

$$f = \frac{[B]}{[A] + [B]} \quad (5)$$

where [B] and [A] represent the integrated areas of the sharp features. From the preceding discussion, it follows that f represents the fraction of ordered, rigid $(C_6H_6)(C_6D_6)_{12}$ clusters in which the unique C_6H_6 chromophore is *not* located in the cluster interior, but rather on the surface.

Two competing hypotheses may be set forth to explain the time-dependent decay of the fraction f. The first proposes that evaporations from rigid $(benzene)_{14}$ are sufficient to describe the data; the second proposes that a subpopulation of ordered, rigid $(benzene)_{13}$ clusters isomerize, where the unique C_6H_6 moiety migrates from the cluster surface to its interior. Both hypotheses presuppose the evaporation dynamics of fluxional clusters (discussed above); at issue is what happens to the ordered, rigid clusters after they have solidified.

1. The Kinetics of Subsequent Evaporation. To investigate whether evaporation from rigid, ordered clusters can account for the observed evolution of *f*, the evaporation reactions that may potentially affect either feature A or feature B in the $(benzene)_{13}$ mass channel must be considered.

	evaporation reaction	timescale (μs)	comments
(v)	$[H][D_{12}] \rightarrow [H][D_{11}] + D$	10^7	
(vi)	$[H][D_{12}]D \rightarrow [H][D_{12}] + D$	130	increases feature A
(vii)	$[D][HD_{11}] \rightarrow [D][D_{11}] + H$	10^7	
(viii)	$[D][HD_{11}] \rightarrow [D][HD_{10}] + D$	10^7	
(ix)	$[D][HD_{11}]D \rightarrow [D][HD_{11}] + D$	130	increases feature B

Using the cluster energies derived by Bartell et al.,[17] evaporation time scales can be estimated within the formalism of eq 3.[16] For reactions vi and ix, where the reactant is $(benzene)_{14}$, only three nearest-neighbor interactions need be overcome and the time scale is relatively short ($\sim$130 μs). This stands in contrast to reactions v, vii, and viii, where the reactant is $(benzene)_{13}$. Because of the large activation energy associated with the $(benzene)_{13}$ closed-shell structure (six nearest-neighbor interactions), rigid $(benzene)_{13}$ clusters at 130 K are stable to evaporation on the 100 μs time scale (evaporation time scale $\sim 10^7$ μs). Thus, the observed evolution in the ratio *f*, if caused by evaporation, must result exclusively from an increase in $(benzene)_{13}$ signal that derives from the evaporation of rigid $(benzene)_{14}$, not from a decrease of signal accompanying evaporation from rigid $(benzene)_{13}$.

Further analysis, however, reveals that the evaporation stoichiometry cannot be reconciled with the data. The two sharp spectral features are initially formed in approximately a 6:5 ratio. On the time scale of the experiment, rigid $[H][D_{12}]D$ may undergo evaporation, increasing the relative intensity of feature A (reaction vi). Remaining rigid $(benzene)_{14}$ clusters may also undergo evaporation, most resulting in the increase of feature B (reaction ix). (When the C_6H_6 moiety is lost to evaporation from $[D][D_{12}]H$, however, the $(benzene)_{13}$ mass channel is not affected.) Consequently, evaporation from rigid $(benzene)_{14}$ will initially affect the spectrum of $(benzene)_{13}$ in approximately the following manner: 55% of rigid $(benzene)_{14}$ evaporations increase the relative area of feature A, 41% increase the relative area of Feature B, and 4% have no effect on the spectrum. Although these considerations predict a gradual decrease in *f* over time, the corresponding reaction rates are physically untenable. If evaporation were the sole mechanism, the data could not be explained unless the fundamental rate of evaporation from rigid $(benzene)_{14}$ were several orders of magnitude faster than the corresponding rate of evaporation from warmer, fluxional $(benzene)_{14}$ clusters.

To quantify this further, the rates of appearance of the features A and B, within the evaporation hypothesis are given by

$$\frac{d[A]}{dt} = ak_f[(HD_{13})_{flux}] + k_r[[H][D_{12}]D] \quad (6)$$

$$\frac{d[B]}{dt} = bk_f[(HD_{13})_{flux}] + k_r[[D][HD_{11}]D] \quad (7)$$

Equation 6 is derived from eq 1 and reaction vi; eq 7 comes from eq 1 and reaction ix. k_r is the rate constant for evaporation from a rigid, ordered $(benzene)_{14}$ cluster. To develop analytical expressions for the time-dependent absorptions of features A and B, we assume that rates of evaporation are approximately equal for neighboring-sized rigid clusters larger than, but not including, $(benzene)_{13}$. (Because of its closed-shell stability, rigid $(benzene)_{13}$ behaves as a "magic number" cluster with respect to evaporation on the time scale of the experiment.)

Derived expressions for the relative integrated areas of features A and B based on the evaporation model are as follows:

$$\frac{[A]_E}{[C]_0} = (ak_r t) + \left(\frac{a}{1-c} - \frac{ak_r}{(1-c)^2 k_f}\right)(1 - \exp(-(1-c)k_f t)) \quad (8)$$

$$\frac{[B]_E}{[C]_0} = \left(\frac{b}{1-c} + \frac{\beta b k_f}{(1-c)k_f - k_r} - \frac{\beta b k_r}{(1-c)^2 k_f - (1-c)k_r}\right) - \left(\frac{\beta b k_f}{(1-c)k_f - k_r}\right)\exp(-k_r t) + \left(\frac{\beta b k_r}{(1-c)^2 k_f - (1-c)k_r} - \frac{b}{1-c}\right)\exp(-(1-c)k_f t) \quad (9)$$

In eq 9, $\beta \approx 0.92$, and corresponds to the fraction of ordered, rigid $[D][HD_{12}]$ that evaporate to yield a C_6D_6 (not C_6H_6) monomer. When eqs 8 and 9 are combined to determine an expression for *f*, a fit to the experimental data is possible, treating *b* and k_r as parameters. (Values of *c*, *d*, and k_f are used as determined above.) The resulting "best-fit" parameters are physically unreasonable. In particular, the hypothetical rate of evaporation from rigid $(benzene)_{14}$, $k_r = 2.5 \times 10^7\ s^{-1} \pm 0.5 \times 10^7\ s^{-1}$. This is 3 orders of magnitude larger than k_f, implying that evaporation from rigid $(benzene)_{14}$ clusters is far more spontaneous than evaporation from fluxional $(benzene)_{14}$.

On the basis of these considerations, we rule out evaporation from rigid $(benzene)_{14}$ as the primary mechanism driving the evolution of *f*. While it is possible, even probable, that background evaporation does occur, a different primary mechanism is required to account for the experimental kinetics.

2. The Kinetics of Subsequent Isomerization. The alternate mechanism advanced to explain the evolution of the fraction *f* involves isomerization of

$$[D][HD_{11}] \rightarrow [H][D_{12}] \quad (x)$$

where, within a subpopulation of 13-clusters, the C_6H_6 moiety migrates from the rigid, ordered cluster's surface to its interior. We designate k_i as the isomerization rate constant for this process. This transformation effects an increase in feature A, directly coupled to a corresponding decrease in feature B.

Analytical expressions for the relative integrated intensities of feature A and feature B, derived within this model, are

$$\frac{[A]_I}{[C]_0} = \left(\frac{a}{1-c} + \frac{bk_f}{(1-c)k_f - k_i} - \frac{bk_i}{(1-c)^2 k_f - (1-c)k_i}\right) - \left(\frac{bk_f}{(1-c)k_f - k_i}\right)\exp(-k_i t) + \left(\frac{bk_i}{(1-c)^2 k_f - (1-c)k_i} - \frac{a}{1-c}\right)\exp(-(1-c)k_f t) \quad (10)$$

$$\frac{[B]_I}{[C]_0} = \frac{bk_f}{(1-c)k_f - k_i}(\exp(-k_i t) - \exp(-(1-c)k_f t)) \quad (11)$$

The expression for *f* is determined from these equations, applying the definition in eq 5. The best (two-parameter) fit of the resulting prediction to the (combined) experimental data is shown in Figure 6. In the figure, the 298 K data are represented

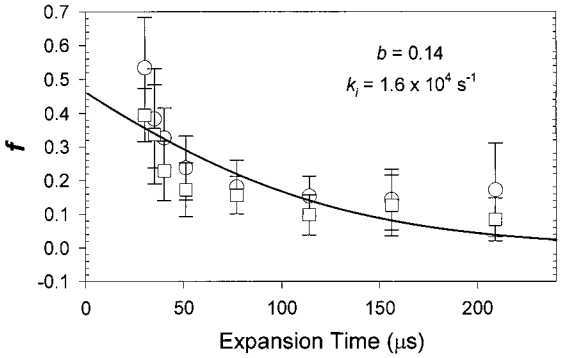

Figure 6. Plot of the fraction, $f = [B]/([A] + [B])$, as a function of expansion time. The 298 K data is represented by circles, 273 K data by squares. The solid line represents a best-fit to the combined data based on the isomerization mechanism. (A similar fit attempted within the evaporation mechanism yields highly nonphysical parameters.) Parameters determined from the isomerization mechanism are $b = 0.14$ and $k_i = 1.6 \times 10^4\ s^{-1}$.

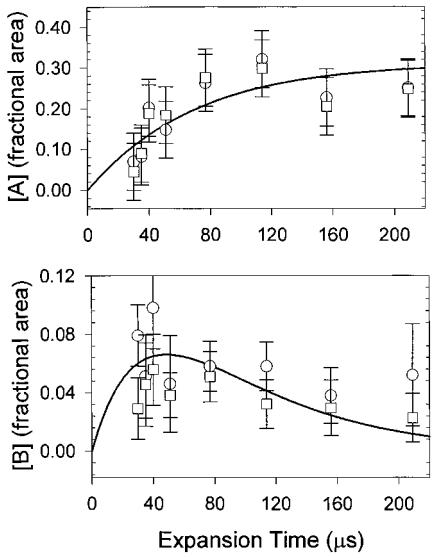

Figure 7. Plot of the fractional integrated areas of feature A (top) and feature B (bottom) as a function of expansion time. The 298 K data is represented by circles, 273 K data by squares. The solid lines correspond to predictions of the isomerization mechanism, determined from eqs 10−11 and the parameters derived in Figures 5 and 6.

by circles and the 273 K data by squares. The analysis yields $b = 0.14 \pm 0.02$, and $k_i = 1.6 \times 10^4\ s^{-1} \pm 0.6 \times 10^4\ s^{-1}$. Because the sum, $a + b + c + d = 1$, and previous analysis gave $c = 0$ and $d = 0.69$, it follows that $a = 0.17$, and the ratio: $a{:}b = 1.2$. The ratio $a{:}b$ is significant because it estimates that the unique C_6H_6 moiety's preference for the rigid, ordered cluster's interior site is ∼15 times greater than what is expected on purely statistical considerations.

As a further validation of eqs 10−11, we have used the parameter values just determined to calculate separately the predicted contributions of these two features to the overall absorption. The results are shown in Figure 7, where the solid lines indicate the model's prediction. In both cases the model's prediction reasonably describes the data.

To summarize, the data suggest that feature A results from ∼17% of fluxional $(benzene)_{14}$ evaporations, while ∼14% of such evaporations result in feature B; the initial appearance of both sharp features occurs on a time scale of ∼35 μs. After their initial appearance, feature B is observed to "transform" into feature A on a longer (∼55 μs) time scale. The experimentally observed time scale, in conjunction with stoichiometric considerations, rules out evaporation from rigid benzene clusters as the primary mechanism.

The isomerization of $[D][HD_{11}]$ to $[H][D_{12}]$ is a direct transformation that affects both feature A and feature B simultaneously. Such an isomerization might involve only a fraction of the energy required to evaporate a molecule from the rigid cluster surface. Furthermore, the preference of C_6H_6 for the center of the $(C_6H_6)(C_6D_6)_{12}$ cluster has been well-documented.[24] These considerations, in concert, lead to the conclusion that isomerization occurs on a time scale of ∼55 μs, resulting in the direct transformation of spectroscopic feature B to feature A.

If eq 3 is used as an approximation to describe the isomerization rate constant, k_i is equivalent to the evaporative rate constant for a process involving the breaking of 3.5 (7.7 kJ) nearest-neighbor interactions in *rigid* $(benzene)_{13}$ at 130 K. Each surface molecule in rigid $(benzene)_{13}$ has a total of six nearest neighbor contacts, so this activation energy is much lower than would be needed for evaporation. A concerted isomerization, the activation of which requires the breaking of three or four nearest neighbor interactions, is a physically realistic mechanism consistent with the data.

Though no theoretical studies to date unambiguously prove the isomerization hypothesis, the proposed mechanism is completely consistent with published theoretical work. It fits well with Bartell's calculations, where it was concluded that benzene clusters in the 13-cluster size range solidify below temperatures of 140 K; between 85 and 140 K, $(benzene)_{13}$ exists in several, rather rigid, equivalent structural isomers, which interconvert.[18] The implication is that not all molecular motion is frozen in the temperature range from 85 to 140 K, even though the clusters are "rigid." Because Bartell's calculations were designed to study an isotopically *homogeneous* system, the specific forces that drive the (C_6H_6) moiety to the cluster interior were not examined. Without inclusion of those driving forces, the specific isomerization we report will not be observed in simulations.

D. Limitations of the Data. As a consequence of the experimental design, the spectrum for only one expansion distance is collected on any given day. While every effort is made to operate under identical conditions, there are unavoidable day-to-day fluctuations, primarily stemming from the laser and from the molecular beam valve. These fluctuations are the primary source of random experimental error in this study and are probably responsible for the majority of scatter that is observed in Figures 5−7. A second experimental complication, the presence of some residual $(C_6H_6)_2(C_6D_6)_{11}$ in the measured $(C_6H_6)(C_6D_6)_{12}$ spectrum, causes a slight overestimation of the integrated area of feature B in all the spectra. The overestimation should be relatively constant, (i.e., independent of expansion distance), so the data is affected most noticeably at the larger expansion distances, where the contribution to feature B from $(C_6H_6)(C_6D_6)_{12}$ is at a minimum. A third potential problem arises from the use of an unskimmed cluster beam, as dictated by physical constraints of the machine (which prevent expansion distance measurements shorter than ∼8 cm when the skimmer is installed). While the use of an unskimmed beam could result in slightly different cluster subpopulations being sampled at different expansion distances, we have not observed any measurable differences between several sets of spectra taken in our lab, differing only by the presence or absence of a skimmer. Though a small overestimation of the integrated intensity of broad feature C at shorter nozzle-to-laser distances cannot be completely ruled out, this appears to be a minor complication

relative to data scatter resulting from day-to-day machine fluctuations (discussed above). In view of these limitations, a brief discussion of the degree of confidence that can be placed in the results is warranted.

Emphasizing that the present report relies to a great extent upon previous experimental results is important. Relevant results have been summarized throughout the discussion, but the supporting data and arguments have not been restated in their original detail. To be specific, results which the present analysis supports (but does not independently prove) include: (1) a high-symmetry, quasi-icosahedral low-energy structure of $(benzene)_{13}$;[22−24] (2) a clear, nonrandom preference of C_6H_6 to occupy the interior site of the $(C_6H_6)(C_6D_6)_{12}$ cluster;[17,24] (3) two distinct, sharp spectral features, one corresponding to C_6H_6 in a surface site (feature B), and one corresponding to C_6H_6 in the cluster interior (feature A);[17,18] and (4) an evolution in feature C over the first 50 μs of expansion, indicative of a nonrigid-rigid cluster transformation occurring in the observed $(benzene)_{13}$ population.[17,18,29] These four conclusions have been in the published record for over half a decade. Together, they constitute a fundamental foundation for the present discussion.

The evolution of f as a function of expansion distance, never before reported, is unambiguously observed in the data. A change in the ratio of the integrated intensities of two spectral features is proportional the change in the relative populations of the physical species responsible for those features. This general principle calls for the conclusion that the population of rigid, ordered clusters with C_6H_6 on the surface (feature B) decreases with time relative to the population of clusters with C_6H_6 in the cluster interior (feature A). As the primary mechanism underlying this population shift, evaporation is eliminated because the required evaporation rate is ~3 orders of magnitude too large, and is not physically realistic. While the isomerization analysis does not provide rigorous proof, isomerization is determined to be consistent with the data; furthermore, the derived rate constant, temperature, and activation energy are all physically reasonable. Given the unavailability of a third mechanism that is both physically realistic and capable of explaining the data, isomerization is the only apparent viable mechanistic option. The experimental observation of isomerization within a molecular 13-cluster is the primary theme of this report.

It almost goes without saying that the level of error associated with the derived kinetic parameters may potentially be reduced using an experimental design that allows for all data collection to be completed in a single day. Based on the present data, it is unwise to place any confidence in spectral differences observed between the two sets of data that differ in their expansion conditions, although one cannot eliminate the eventuality that the (benzene:helium) expansion ratio affects the results. It is certainly worth noting, however, that even the least certain of the kinetic parameters k_f implies an uncertainty in the derived evaporation temperature of only ±2 K; this is because the evaporative rate constant is proportional to $\exp(1/T)$.[29] We further note that the calculated order of magnitude of k_r is sufficient to eliminate evaporation, while the order of magnitude of k_i supports isomerization as the primary mechanism underlying the evolution in f. In summary, even considering all their limitations, the derived kinetic parameters support the general interpretation advanced in this report.

V. Conclusions

We report spectroscopic evidence for isomerization in the $(C_6H_6)(C_6D_6)_{12}$ cluster during free jet expansion, in which the C_6H_6 molecule migrates from the cluster surface to its interior site; these experiments represent the first spectroscopic observation of isomerization in this kind of molecular cluster. The clusters are first generated in fluxional form near 137 K and are then subject to evaporation. Products of $(benzene)_{14}$ evaporation include a significant fraction (~69%) of rigid clusters in a disordered state, along with a ~31% population of ordered, rigid clusters; the majority of the ordered, rigid clusters (~55%) has the unique (C_6H_6) chromophore in the cluster interior. These ratios were found to be relatively insensitive to a tripling of the benzene:helium expansion ratio. Following evaporation/solidification, the subpopulation of rigid clusters having C_6H_6 on the surface isomerizes, with C_6H_6 migrating to the cluster interior. Initial evaporation of fluxional $(benzene)_{14}$ occurs on a time scale of ~35 μs, while subsequent isomerization of rigid $(benzene)_{13}$ takes place on a longer (~55 μs time scale). The latter time scale is consistent with an isomerization mechanism involving the initial "breaking" of 3−4 nearest-neighbor molecular interactions (or equivalent) at 130 K. While background evaporation from rigid $(benzene)_{14}$ cannot be ruled out, such evaporation contributes only insignificantly to the experimental data. These conclusions are fully consistent with extant theoretical studies; nevertheless, unambiguous confirmation will require additional simulations that specifically include the forces responsible for driving the C_6H_6 moiety to the interior of the $(C_6H_6)(C_6D_6)_{12}$ cluster.

The isomerization process, observed for the first time within an intermediate-sized molecular cluster, is of significant interest. Without specific consideration of these results, future theoretical studies designed to elucidate the fundamental nature of the $C_6H_6-C_6D_6$ interactions within isotopically substituted benzene clusters will be hobbled. Eventually, such studies may yield significant new insights into the fundamental nature of nonchemical interactions occurring within isotopically inhomogeneous systems.

Acknowledgment. This research was supported by the Robert A. Welch Foundation [AI-1392]; appreciation is also extended to the donors of the Petroleum Research Fund, administered by American Chemical Society [ACS-PRF Grant 32915-B6] for partial support. Furthermore, the support and assistance of the Chemistry Department and the Office of Research and Sponsored Programs at Southwest Texas State University are gratefully acknowledged.

References and Notes

(1) Hopkins, J. B.; Powers, D. E.; Smalley, R. E. *J. Phys. Chem.* **1981**, *85*, 3739.
(2) Fung, K. H.; Selzle, H. L.; Schlag, E. W. *J. Phys. Chem.* **1983**, *87*, 5113.
(3) Börnsen, K. O.; Selzle, H. L.; Schlag, E. W. *J. Chem. Phys.* **1986**, *85*, 1726.
(4) Börnsen, K. O.; Lin, S. H.; Selzle, H. L.; Schlag, E. W. *J. Chem. Phys.* **1989**, *90*, 1729.
(5) Henson, B. F.; Hartland, G. V.; Venturo, V. A.; Hertz, R. A.; Felker, P. M. *Chem. Phys. Lett.* **1991**, *176*, 91.
(6) Williams, D. E. *Acta Crystallogr.* **1980**, *A36*, 715.
(7) van de Waal, B. W. *J. Chem. Phys.* **1983**, *79*, 3948.
(8) van de Waal, B. W. *Chem. Phys. Lett.* **1986**, *123*, 69.
(9) Hahn, M. Y.; Whetten, R. L. *Phys. Rev. Lett.* **1988**, *61*, 1190.
(10) 10.Adams, J. E.; Stratt, R. M. *J. Chem. Phys.* **1990**, *93*, 1358.
(11) Adams, J. E.; Stratt, R. M. *J. Chem. Phys.* **1996**, *105*, 1743.
(12) Venturo, V. A.; Maxton, P. M.; Felker, P. M. *Chem. Phys. Lett.* **1992**, *198*, 628.
(13) Knochenmuss, R.; Ray, D.; Hess, W. P. *J. Chem. Phys.* **1994**, *100*, 44.
(14) Easter, D. C.; Bailey, L.; Mellott, J.; Tirres, M.; Weiss, T. *J. Chem. Phys.* **1998**, *108*, 6135.

(15) Easter, D. C.; Baronavski, A. P.; Hawley, M. *J. Chem. Phys.* **1993**, *99*, 4942.
(16) Easter, D. C.; Baronavski, A. P.; Hawley, M. *Chem. Phys. Lett.* **1993**, *206*, 329.
(17) Bartell, L. S.; Dulles, F. J. *J. Phys. Chem.* **1995**, *99*, 17100.
(18) Bartell, L. S.; Dulles, F. J. *J. Phys. Chem.* **1995**, *99*, 17107.
(19) Bartell, L. S.; Dibble, T. S., *J. Am. Chem. Soc.* **1990**, *112*, 890.
(20) Bartell, L. S.; Harsanyi, L.; Valente, E. J. *J. Phys. Chem.* **1989**, *93*, 6201.
(21) Del Mistro, G.; Stace, A. J. *Chem. Phys. Lett.* **1990**, *171*, 381.
(22) Easter, D. C.; Li, X.; Whetten, R. L. *J. Chem. Phys.* **1991**, *95*, 6362.
(23) Easter, D. C.; Whetten, R. L.; Wessel, J. E. *J. Chem. Phys.* **1991**, *94*, 3347.
(24) Easter, D. C.; Khoury, J. T.; Whetten, R. L. *J. Chem. Phys.* **1992**, *97*, 1675.
(25) Kang, W. K.; Kim, E. J.; Choi, C. J.; Jung, K. W.; Jung, K.-H. *Bull. Kor. Chem. Soc.* **1995**, *16*, 238.
(26) Kay, B. D.; Raymond, T. D.; Rice, J. K. *Rev. Sci. Instrum.* **1986**, *57*, 2266.
(27) Lubman, D. Private communication.
(28) Klots, C. E. *J. Phys. Chem.* **1988**, *92*, 5864.
(29) Klots, C. E. *Z. Phys. D.* **1991**, *20*, 105.